

Novel Linearization Architecture with Limited ADC Dynamic Range for Green Power Amplifiers

Ying Liu, *Member, IEEE*, Chuang Huang, *Member, IEEE*, Xin Quan, *Student Member, IEEE*,
Patrick Roblin, *Senior Member, IEEE*, Wensheng Pan, and Youxi Tang

Abstract—Design of high-efficiency power amplifier (PA) is one of the key challenges to realize green radios, wherein digital predistortion (DPD) is deployed to reduce the PA’s power back-off and thus increase its power efficiency. As the bandwidth of the transmit signal increases, stringent requirements are posed on the DPD linearization performance with limited sampling rate and dynamic range for the analog-to-digital converter (ADC) in the DPD feedback channel. In this paper, under a fixed ADC sampling rate, novel DPD architecture is proposed to compensate for the PA nonlinearity with limited ADC dynamic range. In the feedback channel of the proposed architecture, an extra radio frequency (RF) cancellation chain is introduced to eliminate the linear component of the PA amplified signal, and thus the requirement on the ADC dynamic range can be significantly reduced. Subsequently, by accurately estimating the loop delay and attenuation of the cancellation chain, the baseband replica of the RF cancelling signal is recovered, and the original PA output signal is rebuilt to estimate the DPD coefficients. Finally, experiments show that for the long term evolution (LTE)-advanced signals, the proposed architecture can achieve an adjacent channel leakage ratio lower than -47.6 dBc, which outperforms the conventional DPD by about 3.4 dB, with the effective bits of the ADC being reduced by 4.4 and a power added efficiency of 43.8% with 7.3 dB power back-off being observed for a fabricated Doherty PA with 50 -dBm saturation power.

Index Terms—Green communication, high-efficiency power amplifier, digital predistortion (DPD), dynamic range, nonlinearity.

I. INTRODUCTION

IN ORDER to provide high transmission rates and wide-band access to the exponentially increasing service subscribers, high bandwidth-efficiency protocols, e.g., orthogonal frequency division multiplexing (OFDM), are widely employed in modern digital wireless communication systems [1]. Suffered from high peak to average power ratios (PAPR) of these modulated signals [2], power

Manuscript received August 1, 2015; revised December 27, 2015 and April 17, 2016; accepted June 28, 2016. Date of publication August 16, 2016; date of current version December 29, 2016. This work was supported in part by the National Natural Science Foundation of China under Grant 61531009, Grant 61271164, Grant 61471108, Grant 61501093, and Grant 61201266, in part by the National Major Projects under Grant 2014ZX03003001-002, and in part by the Fundamental Research Funds for the Central Universities. (*Corresponding author: Chuang Huang*.)

Y. Liu, C. Huang, X. Quan, W. Pan, and Y. Tang are with the National Key Laboratory of Science and Technology on Communications, University of Electronic Science and Technology of China, Chengdu 611731, China (e-mail: liuying850613@uestc.edu.cn; huangch@uestc.edu.cn).

P. Roblin is with the Department of Electrical and Computer Engineering, The Ohio State University, Columbus, OH 43210 USA (e-mail: roblin.1@osu.edu).

Color versions of one or more of the figures in this paper are available online at <http://ieeexplore.ieee.org>.

Digital Object Identifier 10.1109/JSAC.2016.2600415

0733-8716 © 2016 IEEE. Translations and content mining are permitted for academic research only. Personal use is also permitted, but republication/redistribution requires IEEE permission. See http://www.ieee.org/publications_standards/publications/rights/index.html for more information.

amplifiers (PAs) are consequently required to work with large power back-off to preserve the linearity of the transmit signal [3]; otherwise, the PA’s inherent nonlinearity will result in severe in-band distortion and spectral regrowth, i.e., spectral broadening due to the inter-modulation, which significantly deteriorate the adjacent channel leakage ratio (ACLR) of the transmitted signal and the bit error rate (BER) at the receiver [4]. Unfortunately, large power back-off dramatically brings down the power efficiency of the PA, which leads to considerable waste of energy at the base stations (BSs) [3]. On the other hand, PA is the biggest single consumer for energy among all the hardware components at the BS, and it is estimated that [5] it consumes as much as $50\% \sim 80\%$ of the electricity expended at the BS. Therefore, how to boost the PA’s power efficiency is the most crucial issue to realize the green wireless radios.

Aiming to increase the power efficiency while preserving reasonable linearity of a PA, the Doherty PA equipped with digital predistortion (DPD) technique had been studied recently in the literatures [6]–[8]. In the conventional DPD architectures, a high performance feedback channel was required to down-convert, filter, and digitalize the PA output signal, which consequently poses stringent requirements on both the sampling rate and dynamic range of the analog-to-digital converter (ADC) and the bandwidth of the associated radio frequency (RF) filters [9]. In general, due to the PA nonlinearities, the bandwidth of the PA output signal would be expanded to about five times of that for the input signal [10]. In order to accurately capture the feedback signal with such a wide bandwidth, e.g., 100 MHz for the LTE-advanced signals, the DPD feedback channel employed the RF filters with over 500 MHz bandwidth and ADCs with sampling rate over 1000 mega-samples per second (MSPS) [11]. However, under the constraints of implementation cost and power consumption, it is unaffordable and impractical to deploy ADCs with satisfactory dynamic range at such a high sampling rate [10], [12], [13]. Furthermore, higher dynamic ranges and sampling rates usually imply higher power consumption [16], which goes against the principle of green communications. For instance, a typical power consumption for a 12-bit ADC12D500 [14] is approximately 44.3% higher than that for a 8-bit ADC08D500 [15] with the same sampling rate. As such, the tradeoff between the sampling rate and the dynamic range of the ADC needs to be carefully investigated in the design of green PAs.

Recently, a lot of works were dedicated to the studies of the architectures and algorithms for DPD [4], [9]–[11], [17]–[19],

addressing the performance degradation caused by the restrictions of the hardware, such as the sampling rate limitation on the ADC [9], [11], [17]. Only a few works in the literatures [18], [19] had analyzed the impact of a limited ADC dynamic range, where the authors investigated the effects of quantization on linearization performance of the look-up-table based [19] and adaptive direct learning DPD [18]. The above results could be applied to determine the optimal dynamic range of an ADC for the DPD linearization based on the knowledge of the characteristic of the RF amplifier and the maximum allowable adjacent-channel interference (ACI). However, no in-depth studies had been devoted to mitigating the effect of limited ADC dynamic range on wide-band PAs, particularly when the requirements on both the ADC sampling rate and dynamic range need to be strictly satisfied, e.g., for the scenarios of LTE-advanced signals with carrier aggregation [3], [5], [9], [10], [20].

In this paper, a novel DPD architecture with limited ADC dynamic range at a fixed sampling rate is proposed to effectively compensate for the nonlinear distortions caused by PA of wide-band stimulus. The contributions of this paper are briefly summarized as follows.

- 1) The proposed DPD architecture consists of a RF signal cancellation chain and a baseband signal reconstruction module, where the former mitigates the linear component of the PA output signal to reduce the dynamic range and the latter recovers the original PA output signal from the residual signal after the cancellation operation.
 - a) *RF Cancellation*: For the design of the RF cancellation chain, two options are proposed: the RF and baseband tuning schemes. The RF tuning scheme taps the transmit signal before the PA to generate a RF cancelling signal, and the baseband tuning scheme generates it directly from the baseband source signal. In essence, the two schemes are equivalent, while the baseband tuning scheme is easier to be implemented. Differently, the RF scheme requires some dedicated RF devices to adjust the delay and amplitude of the cancelling signal; and the baseband scheme adjusts these parameters in digital domain and thus can be easily implemented.
 - b) *Baseband Reconstruction*: After acquiring the residual signal with limited dynamic range, the signal reconstruction operation is adopted to rebuild the original PA output signal. By accurately estimating the loop delay and attenuation of the RF cancellation chain, a baseband replica of the RF cancelling signal is generated to reconstruct the PA output signal from the residual signal, base on which PA model extraction and DPD linearization are accomplished.
- 2) The impacts of the loop delay and attenuation estimation errors on the performance of the signal reconstruction and PA model extraction are also analyzed. A closed-form expression for the reconstructed signal is derived, wherein the estimation errors contribute to deviate the reconstructed signal from the original PA output signal

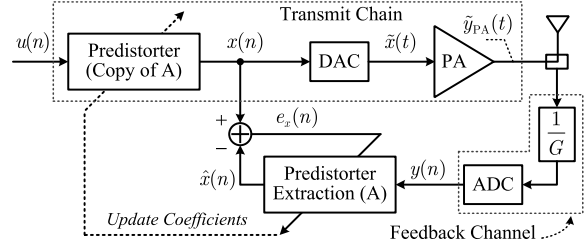


Fig. 1. Conventional DPD with indirect learning structure [21].

and the variance of the deviation is also analyzed. Moreover, a closed-form expression for the normalized mean square error (NMSE) on the PA model extraction is derived in terms of the root mean square (RMS) values of the estimation errors, the transmit signal bandwidth, and the signal-to-noise ratio (SNR) of the feedback channel.

- 3) Finally, experiments are performed on LTE-advanced signals to demonstrate the effectiveness of the proposed DPD architecture as well as the efficiency improvement on a widely-used Doherty PA. The modeling and linearization performance clearly shows that the proposed DPD architecture can effectively mitigate the nonlinear distortion for PAs, even when the resolution (the total number of bits) of the ADC are reduced from 12 bits to 8 bits. A power efficiency of 43.8% is observed at the output power level of 42.7 dBm with -45 dBc ACLR performance for a Doherty PA with saturation power of 50 dBm.

This paper is organized as follows. First, in Section II, the conventional DPD linearization operations are described. Then, the proposed DPD model coefficients estimation with limited ADC dynamic range is described in Section III. Next, Section IV presents some analysis closely related to the proposed architecture and Section V presents the experimental results. Finally, Section VI concludes this paper.

II. PROBLEM STATEMENT

First, this section briefly introduces the conventional DPD linearization architecture. Then, the requirements on the dynamic range of the ADC in the DPD feedback channel are reviewed.

A. Conventional DPD

Fig. 1 shows the architecture of a typical DPD [4] with the indirect learning structure [21] adopted for DPD coefficient extraction, which consists of three major components: the transmit chain, the feedback channel, and the predistorter extraction module.

In the transmit chain, the baseband source signal $u(n)$ is the input of the digital predistorter module, and the predistorted signal $x(n)$ is subsequently processed by the DAC and up-converted to RF signal $\tilde{x}(t)$ which is then fed into the PA for amplification and transmission. It is noticed that at the beginning of the DPD model extraction, the predistorter module does not work, and it follows $x(n) = u(n)$.

In the feedback channel, the PA output signal $\tilde{y}_{PA}(t)$ is attenuated by a factor of G , and sampled by the ADC to

obtain the equivalent baseband replica of $\tilde{y}_{\text{PA}}(t)$, i.e., $y(n)$. Then, the signals $y(n)$ and $x(n)$ are aligned in the time domain and normalized in power before being sent to the predistorter extraction module (block A in Fig. 1) to estimate parameters of the DPD model.

The predistorter extraction module utilizes the PA feedback signal $y(n)$ as its input and $\hat{x}(n)$ as its output. The predistorter module (copy of block A) is an exact copy of the predistorter extraction module. The objective of this indirect learning structure is to tune block A to minimize the power $|e_x(n)|^2$ of the error signal $e_x(n) \triangleq x(n) - \hat{x}(n)$ [21]. In particular, by assuming the characteristic of the PA nonlinear behavior is invertible [4], the indirect learning structure can obtain parameters for block A to ensure $e_x(n) = 0$, i.e., the PA nonlinearities is perfectly counteracted as $y(n) = u(n)$.

B. Math Models

In general, a real PA device can be approximated by Volterra series [4]. However, the high computational complexity in the Volterra series makes it unattractive for implementation. In order to demonstrate the idea of DPD, a simplified PA model is adopted by using the power series, i.e.,

$$\tilde{y}_{\text{PA}}(t) = \tilde{f}(\tilde{x}(t)) = \sum_{k=1}^K \tilde{b}_k \tilde{x}^k(t), \quad (1)$$

where $\tilde{f}(\cdot)$ denotes the pass-band PA function, and \tilde{b}_k is the real-valued coefficient for the k -th order power series. Memory effect can also be easily included in (1) by adding more groups of similar series with $\tilde{x}(t)$ being replaced by $\tilde{x}(t-\tau)$, where τ represents the time span a PA can memorize its input. Conventionally, it is equivalent to analyze the PA behavior in baseband and a memory-polynomial (MP) model can be obtained by mapping the simplified PA model in (1) to baseband, i.e.,

$$y(n) = f(x(n)) = \sum_{k=0}^{K-1} \sum_{q=0}^{Q-1} w_{kq} x(n-q) |x(n-q)|^k, \quad (2)$$

where $f(\cdot)$ denotes the equivalent baseband PA function, w_{kq} is the MP-based PA complex coefficient for k -th order and q -th memory depth.

In the indirect learning structure, the predistorter module is assumed to have the same model as the PA. Thus, by simply swapping the input and output in (2), the DPD model is expressed as

$$x(n) = f(y(n)) = \sum_{k=0}^{K-1} \sum_{q=0}^{Q-1} \omega_{kq} y(n-q) |y(n-q)|^k, \quad (3)$$

where ω_{kq} is the DPD model complex coefficient for k -th order and q -th memory depth.

Correspondingly, by constructing the same model as (3) on source signal $u(n)$ and copying the parameters ω_{kq} to the predistorter module, the DPD linearization operation is then initiated. After being processed by the predistorter module, the

predistorted source signal can be written as

$$x_{\text{DPD}}(n) = f(u(n)) = \sum_{k=0}^{K-1} \sum_{q=0}^{Q-1} \omega_{kq} u(n-q) |u(n-q)|^k, \quad (4)$$

which is then sent to the PA to counteract the nonlinear distortion.

C. Requirement for ADC Dynamic Range

As described in detail in [4], the conventional DPD linearization has been proved to be an effective method to mitigate PA nonlinearity, and then spectral regrowth and adjacent channel interference (ACI) can be significantly suppressed. The effectiveness of the conventional DPD linearization heavily lays in the fact that the requirements for both the sampling rate and dynamic range of the ADC are satisfied simultaneously.

Analyzing the impact of the ADC quantization on DPD linearization is important, and one can determine the optimal ADC dynamic range to achieve a given linearization performance. The dynamic range of an ADC, defined as the ratio of the maximum signal power to the minimum signal power that can be reliably measured simultaneously, is generally limited by the number of bits of the selected ADC [22]. When the minimum signal power equals the quantization noise power of the full-scale input signal, the dynamic range can be estimated from the signal to quantization noise ratio of an ideal ADC with N bits as $\eta_{\text{DR}} = 6.02 \times N + 1.76$. In order to further include the nonlinear distortion effects of the sampling process, ENOB is usually adopted to characterize the practical ADC resolution instead of the stated number of bits listed in the product specifications [16]. Therefore, considering both the quantization error and distortion effects introduced during the sampling process, the dynamic range η_{DR} is expressed in terms of ENOB b_{ENOB} as $\eta_{\text{DR}} = b_{\text{ENOB}} \times 6.02 + 1.76$ [23]. For a wide-band signal with a given maximum ACI σ_{ACI} , the ENOB of the ADC is approximately derived from [18] as

$$b_{\text{ENOB}} \approx \frac{\gamma_{\text{ADC}} - 1.76 + 10 \log_{10} r_{\text{PAPR}}}{6.02},$$

where r_{PAPR} is the estimated PAPR of the acquired signal, defined as the ratio between the maximum instantaneous power of the acquired signal and its average power, and γ_{ADC} is the SNR of the quantized signal calculated by [19]

$$\gamma_{\text{ADC}} = \frac{2B_{\text{eq}}}{f_s \sigma_{\text{ADC}}},$$

with f_s being the sampling rate and B_{eq} being the noise bandwidth. For the design of the DPD feedback channel, due to the spectral broadening, the sampling bandwidth should be equal to the noise bandwidth [18], i.e., $2B_{\text{eq}}/f_s = 1$.

For instance, when -70 dBc ACI is required [24], the SNR of the quantized signal γ_{ADC} is about 70 dB, and thus an ADC with ENOB of at least $b_{\text{ENOB}} = 13$ bits is required. In practice, considering the noise and distortion introduced by ADC, the actual ADC bit-width (resolution) are in general $2 \sim 3$ bits more than the ENOB. Recently,

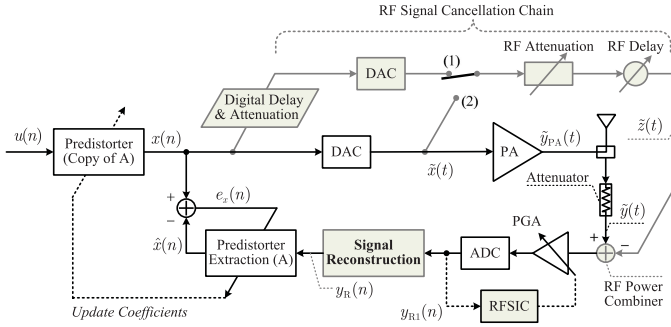


Fig. 2. The block diagram of the proposed DPD architecture with limited ADC dynamic range. An RF signal cancellation chain is implemented either by tapping the signal in baseband domain or RF domain to cancel the linear component of the PA output signal. A signal reconstruction module is utilized to recover the PA output signal from the residual signal after the RF cancellation.

an evaluation board, namely TI TSW1266, is designed for wide-band LTE-advanced linearization applications with bandwidth up to 100 MHz. In order to meet the ACLR requirement of -45 dBc [25], a 12-bit ADC with an ENOB of 9.8 bits is deployed to digitalize the PA output signal for the BS [26]. As the transmission bandwidth and ACLR requirement increase, limited ADC dynamic range becomes a key obstacle for the effective linearization of PA.

III. THE PROPOSED DPD ARCHITECTURE

The main idea of the proposed architecture is to utilize an additional RF signal cancellation chain to subtract the linear component of the PA output signal, and thus the ADC in the feedback channel only needs to capture the residual signal, resulting in much smaller ADC dynamic range. Subsequently, a signal reconstruction operation is adopted to rebuild the original PA output signal from a baseband replica of the RF cancelling signal which is generated based on accurately estimating the loop delay and attenuation of the RF cancellation chain. Under the proposed architecture, the ADC dynamic range is reduced while achieving similar linearization performance.

The block diagram of the proposed DPD architecture is presented in Fig. 2, in which the RF signal cancellation chain and the signal reconstruction module are shown in gray block. The RF cancellation chain provides two options, i.e., the RF tuning scheme and the baseband tuning scheme, to generate a RF cancelling signal synchronized in time and normalized in power with the PA output signal with a 180-degree phase difference.

- 1) *RF tuning scheme*: the RF cancelling signal is generated by tapping the transmit signal before the PA where its delay and attenuation are adjusted by dedicated RF devices.
- 2) *Baseband tuning scheme*: the RF cancelling signal is generated by transmitting an digitally attenuated and delayed replica of the baseband source signal with an extra transmit circuit.

In essence, the RF tuning and baseband tuning schemes are identical and can achieve the same cancelling performance.

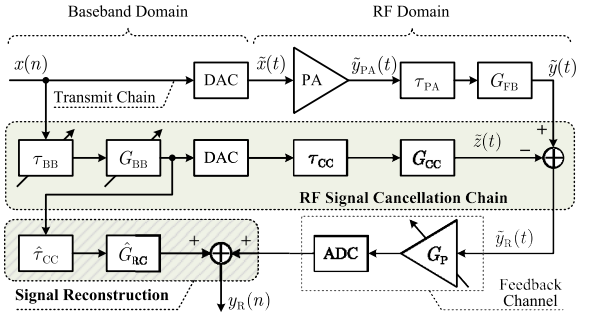


Fig. 3. The block diagram of the proposed RF signal cancellation chain (the dashed box), the signal reconstruct module (the dashed box with diagonal stripes), the transmit train, and the feedback channel.

However, for the latter, the delay and attenuation tuning operations can be easily implemented in digital domain by adjusting the group delay and amplitude of the transmit signal with high accuracy [27], [28]. Thus, to simply demonstrate the effectiveness of the proposed DPD architecture, only the baseband tuning scheme is analyzed in this paper.

To clearly illustrate the proposed RF signal cancellation and reconstruction architecture, an equivalent block diagram including the transmit chain, the feedback channel, the RF signal cancellation chain and the signal reconstruction module, is shown in Fig. 3, where the proposed RF signal cancellation chain is illustrated in the dashed box and the signal reconstruction module is illustrated in the dashed box with diagonal strips. In the rest of this section, the signal cancellation, signal reconstruction, and DPD linearization operations in the proposed DPD architecture are respectively introduced.

A. Signal Cancellation

As illustrated in Fig. 3, the RF signal cancellation chain consists of several major components: the digital loop delay module, the attenuation module, an extra DAC, and a power combiner. Before showing how it works, we first define some notations of the proposed architecture: Let τ_{TC} denote the loop delay from the DAC in the transmit chain to the ADC in the feedback channel, and τ_{CC} represents the overall loop delay from the DAC in the cancellation chain to the ADC in the feedback channel. τ_{BB} and G_{BB} are the variable delay and attenuation tuned to cancel the linear component of the PA output, which are also shared with the signal reconstruction module. G_{FB} is the attenuator in the feedback channel. G_P is the variable gain of the programmable gain amplifier (PGA) in the feedback channel used to amplify the RF residual signal $\tilde{y}_R(t)$ before entering the ADC.

The proposed cancellation and reconstruction operations are described as follows. First, we turn off the RF cancellation and the reconstruction chains by setting $G_{BB} = 0$, and thereby the system works the same as a conventional DPD. The PGA is programmed to be $G_P = G_{P0}$ to ensure the input signal of the ADC reaches a power level lower than the ADC saturation power by a certain value, e.g., 10 dB for LTE-advanced signals with 10 dB PAPR. In the digital domain, the residual signal

after the ADC sampling is given as

$$y_{R0}(n) = G_{P0}y(n) = G_{P0}G_{FB}y_{PA}\left(n - \frac{\tau_{TC}}{T}\right), \quad (5)$$

where $y_{R0}(n)$ denotes the ADC captured sample without RF cancellation, T is the ADC sampling time interval, and $y_{PA}(n) = \tilde{y}_{PA}(nT)$ is the baseband equivalent for the PA output signal $\tilde{y}_{PA}(t)$. The power $\mathbb{E}[|y_{R0}(n)|^2]$ of the digitalized residual signal $y_{R0}(n)$ is recorded for power normalization in the following operations, where $\mathbb{E}[\cdot]$ denotes the expectation.

Then, we turn on the cancellation and reconstruction chains and tune $G_{BB} \triangleq G_{FB}\tilde{b}_0/G_{CC}$. The RF output signal of the RF power combiner (shown in Fig. 3) can be rewritten as

$$\tilde{y}_{R1}(t) = \tilde{y}(t) - \tilde{z}(t), \quad (6)$$

where

$$\tilde{z}(t) \triangleq G_{CC}G_{BB}\tilde{x}(t - \tau_{BB} - \tau_{CC}) \quad (7)$$

is the RF cancelling signal directly generated from the baseband signal $x(n)$, i.e., $\tilde{z}(nT) = G_{CC}G_{BB}x\left(n - (\tau_{BB} + \tau_{CC})/T\right)$. Recalling the pass-band PA model given in (1), the residual RF signal at the power combiner output can be written as

$$\begin{aligned} \tilde{y}_{R1}(t) &= G_{FB}\tilde{f}(\tilde{x}(t - \tau_{TC})) - \tilde{z}(t) \\ &= G_{FB}\tilde{b}_0\tilde{x}(t - \tau_{TC}) - G_{CC}G_{BB}\tilde{x}(t - \tau_{BB} - \tau_{CC}) \\ &\quad + G_{FB}\tilde{f}_{ND}(\tilde{x}(t - \tau_{TC})), \end{aligned} \quad (8)$$

where $\tilde{f}_{ND}(\tilde{x}(t - \tau_{TC})) = \sum_{k=2}^K \tilde{b}_k \tilde{x}^k(t - \tau_{TC})$. In the cancellation chain, when the attenuation and the delay are closely matched with those of the transmit chain, i.e., $G_{BB} \approx G_{FB}\tilde{b}_0/G_{CC}$ and $\tau_{BB} \approx \tau_{TC} - \tau_{CC}$, the linear component of the PA amplified signal can be mostly eliminated [27], [29]–[31], i.e., $G_{FB}\tilde{b}_0\tilde{x}(t - \tau_{TC}) - G_{CC}G_{BB}\tilde{x}(t - \tau_{BB} - \tau_{CC}) \approx 0$. Then, the residual RF signal at the power combiner output becomes

$$\tilde{y}_{R1}(t) \approx G_{FB}\tilde{f}_{ND}(\tilde{x}(t)) = \sum_{k=2}^K \tilde{b}_k \tilde{x}^k(t), \quad (9)$$

whose average power is significantly reduced, compared to that of the original RF feedback signal $\tilde{y}(t)$.

Remark 1: By subtracting $\tilde{b}_0\tilde{x}(t)$ from the PA output signal $\tilde{y}_{PA}(t) = \tilde{b}_0\tilde{x}(t) + \sum_{k=2}^K \tilde{b}_k \tilde{x}^k(t)$, the decreasing of the dynamic range for the residual signal is approximately equal to the power value of the subtracted linear component, i.e. $\mathbb{E}[\tilde{b}_0^2 \tilde{x}^2(t)]$. Correspondingly, the dynamic range of the ADC is reduced by about $\mathbb{E}[\tilde{b}_0^2 \tilde{x}^2(t)]$. For example, in the conventional advanced Doherty PA designs [6], [7], an ACLR performance lower than -30 dBc can be achieved, i.e., the linear component of the PA output $\tilde{b}_0\tilde{x}(t)$ is approximately 30 dB larger than the distortion components $\sum_{k=2}^K \tilde{b}_k \tilde{x}^k(t)$ [32]. Thus, by applying the proposed cancellation scheme, an ADC dynamic range of approximately 30 dB can be reduced.

Remark 2: For applications with the dynamic range of the signal-of-interest beyond that of a selected ADC, it is more convenient to extend Remark 1 to cover the dynamic range expansion of the ADC achieved by the signal cancellation architecture. By applying the signal cancellation, the power level of the residual signal is reduced within the dynamic

range of the ADC. Then, in order to take full advantage of all the ADC resolution bits, the residual signal is amplified by the PGA to approach the maximum input range of the ADC. In such cases, the dynamic range of the ADC is equivalently expanded by a value equal to the dynamic range reduction of the PA output signal.

Therefore, to ensure the maximum power of the residual RF signal $\tilde{y}_{R1}(t)$ approaches the maximum input range of the ADC, PGA is programmed with $G_P = G_{P1}$ to further amplify the residual signal before entering the ADC. After ADC sampling, $\tilde{y}_{R1}(t)$ is digitalized to $y_{R1}(n)$ with

$$\begin{aligned} y_{R1}(n) &= G_{P1}(\tilde{y}(nT) - \tilde{z}(nT)) = G_{P1}G_{FB}\tilde{y}_{PA}(nT - \tau_{TC}) \\ &\quad - G_{P1}G_{CC}G_{BB}\tilde{x}(nT - \tau_{BB} - \tau_{CC}). \end{aligned} \quad (10)$$

To obtain the baseband model for the RF signal cancellation operation, both $\tilde{y}_{PA}(nT - \tau_{TC})$ and $\tilde{x}(nT - \tau_{BB} - \tau_{CC})$ are replaced by their baseband equivalents, respectively, i.e.,

$$\begin{aligned} y_{R1}(n) &= G_{P1}G_{FB}y_{PA}\left(n - \frac{\tau_{TC}}{T}\right) \\ &\quad - G_{P1}G_{CC}G_{BB}x\left(n - \frac{\tau_{BB} + \tau_{CC}}{T}\right). \end{aligned} \quad (11)$$

To quantify the relaxation on the ADC dynamic range requirement, a definition concerning a selected ADC using the proposed architecture to improve its dynamic range is given as follows.

Definition 1: Define the ADC dynamic range improvement (DRI) as

$$G_{DRI} = \frac{G_{P1}}{G_{P0}}, \quad (12)$$

where G_{P0} is the initial gain of the PGA without RF cancellation and G_{P1} is the gain of the PGA after cancellation, defined as

$$G_{P1}^2 = \frac{G_{P0}^2 \mathbb{E}[\tilde{y}_{R0}^2(t)]}{\mathbb{E}[\tilde{y}_{R1}^2(t)]} = \frac{G_{P0}^2 \mathbb{E}[|y_{R0}(n)|^2]}{\mathbb{E}[|y_{R1}(n)|^2]}. \quad (13)$$

Since the power of the feedback RF signal without RF cancellation $\tilde{J} = \mathbb{E}[\tilde{y}_{R0}^2(t)] = \mathbb{E}[|y_{R0}(n)|^2]$ is fixed, the DRI maximization problem is equivalent to minimize the power of the received feedback signal after RF cancellation, i.e.,

$$\begin{aligned} \min_{\{\tau_{BB}, G_{BB}\}} J \\ = G_{P1}^2 \mathbb{E} \left[\left| G_{FB}y_{PA}\left(n - \frac{\tau_{TC}}{T}\right) - G_{CC}G_{BB}x\left(n - \frac{\tau_{BB} + \tau_{CC}}{T}\right) \right|^2 \right]. \end{aligned} \quad (14)$$

By exploiting brutal searching procedure over a two dimensional parameter space defined by τ_{BB} and G_{BB} , e.g., $-2T_s \leq \tau_{BB} - \tau_{TC} + \tau_{CC} \leq 2T_s$ and $-0.2V \leq G_{BB} - G_{FB}\tilde{b}_0/G_{CC} \leq 0.2V$, the delay τ_{BB} and attenuation G_{BB} can be obtained, i.e., $\tau_{BB} = \tau_{TC} - \tau_{CC}$ and $G_{BB} = G_{FB}\tilde{b}_0/G_{CC}$.

Fig. 4 shows the DRI performance versus the delay and attenuation estimation errors, i.e., $(\tau_{TC} - \tau_{CC}) - \tau_{BB}$ and $G_{FB}\tilde{b}_0/G_{CC} - G_{BB}$. In the simulation, the MP model in [4] is adopted to simulate a real PA, which nonlinearly distorts the 20 MHz LTE-advanced signal with ACLR being -30 dBc. A maximum DRI of 28 dB is achieved with the delay τ_{BB}

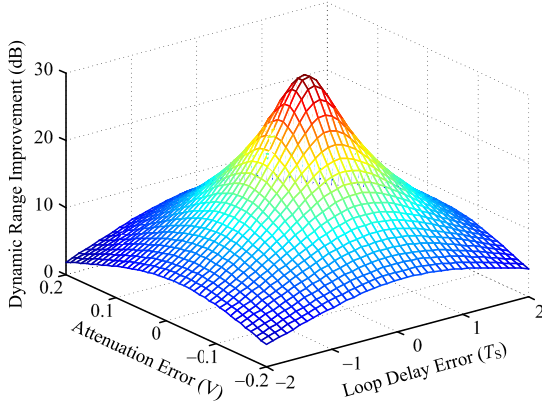


Fig. 4. Dynamic range improvement in terms of the loop delay and attenuation estimation errors $(\tau_{\text{TC}} - \tau_{\text{CC}}) - \tau_{\text{BB}}$ and $G_{\text{FB}}\tilde{b}_0/G_{\text{CC}} - G_{\text{BB}}$.

and attenuation G_{BB} closely matched with the loop delay and attenuation of the RF cancellation chain, i.e., $\tau_{\text{BB}} = \tau_{\text{TC}} - \tau_{\text{CC}}$ and $G_{\text{BB}} = G_{\text{FB}}\tilde{b}_0/G_{\text{CC}}$.

Due to the signal cancellation, the dynamic range requirement on the ADC can be relaxed by a maximum of 28 dB. Consequently, with a simple calculation, the ENOB is verified to be reduced by approximately $28/6.02 \approx 4.7$ bits which relaxes the restriction on ADC selection. Equivalently, for a selected ADC, the dynamic range can also be improved by about 28 dB, i.e., the ENOB of the ADC can be extended by about 4.7 bits. E.g., for a 12-bit ADC with an ENOB of 9.8 bits, by applying the signal cancellation, the ENOB can be further extended to 14.5 bits, which can accommodate signals with a maximum dynamic range of approximately $14.5 \times 6.02 + 1.76 \approx 89.1$ dB.

B. Signal Reconstruction

In order to characterize the nonlinear behavior of the PA and linearize it, the PA output should be accurately estimated. However, in the proposed architecture, only part of the signal (the residual signal after removing the linear component) is available after the ADC sampling process, with which it is difficult to estimate the PA and DPD models. As such, in the digital domain, a baseband replica of the RF cancelling signal is first generated by accurately estimating the delay and attenuation of the RF cancellation chain. Then, the PA output signal is reconstructed by adding the baseband cancelling signal to the residual signal, and thus the DPD parameters can be estimated.

1) Delay Estimation: During the RF cancellation process, τ_{BB} was tuned to $\tau_{\text{BB}} = \tau_{\text{TC}} - \tau_{\text{CC}}$ to ensure that the RF cancelling signal is aligned in time with the PA output signal at the power combiner. Correspondingly, during the signal recovering process, the loop delay τ_{CC} should be estimated to ensure that the baseband cancelling signal is aligned in time with the baseband residual signal. By applying the cross-correlation method [28] on the initial feedback signal $y_{\text{R}0}(n)$ without RF cancellation and the PA input signal $x(n)$, the loop delay τ_{TC} for the transmit chain can be estimated as

$$\hat{\tau}_{\text{TC}} = \arg \max_{\{-L+1 \leq m \leq L+1\}} |R_{yx}(m)|, \quad (15)$$

where $R_{yx}(m)$ is defined as [28]

$$R_{yx}(m) = \begin{cases} \frac{1}{L} \sum_{n=0}^{L-m-1} y(n+m)x^*(n), & m \geq 0 \\ \frac{1}{L} \sum_{n=0}^{L-m-1} y^*(n-m)x(n), & m < 0 \end{cases}, \quad (16)$$

$-L+1 \leq m \leq L+1$, and L being the length of samples over which the cross-correlation operation is taken. Then, the loop delay of the RF cancellation chain is estimated as $\hat{\tau}_{\text{CC}} = \hat{\tau}_{\text{TC}} - \tau_{\text{BB}}$, and thus the baseband replica of the RF cancelling signal $\hat{x}(n)$ is rebuilt as

$$\hat{x}(n) = \hat{G}_{\text{RC}}G_{\text{BB}}x\left(n - \frac{\tau_{\text{BB}} + \hat{\tau}_{\text{CC}}}{T}\right), \quad (17)$$

where $\hat{G}_{\text{RC}} = G_{\text{P}} \times \hat{G}_{\text{CC}}$ is the estimated attenuation for G_{RC} with $G_{\text{P}} = G_{\text{P}1}$.

2) Attenuation Estimation: To estimate the attenuation of the RF cancellation chain G_{CC} , an additional step is needed, i.e., turning off the transmit chain while maintaining the function of the RF cancellation chain. The PGA is programmed to be $G_{\text{P}} = G_{\text{P}2}$ to ensure the RF cancelling signal $\tilde{z}(t)$ utilizes all the ENOB of the ADC to minimize the quantization noise power of the ADC and reduce its effect on the power estimation of the RF cancelling signal. As such, after ADC sampling, the digitized RF cancelling signal $y_{\text{R}2}(n)$ is given as

$$y_{\text{R}2}(n) = G_{\text{P}2}\tilde{z}(nT). \quad (18)$$

By replacing the baseband equivalent of $\tilde{z}(nT)$, $y_{\text{R}2}(n)$ is rewritten as

$$y_{\text{R}2}(n) = G_{\text{P}2}G_{\text{CC}}G_{\text{BB}}x\left(n - \frac{\tau_{\text{BB}} + \tau_{\text{CC}}}{T}\right), \quad (19)$$

with its power being $\mathbb{E}[|y_{\text{R}2}(n)|^2] = G_{\text{P}2}^2G_{\text{CC}}^2G_{\text{BB}}^2\mathbb{E}[|x(n - (\tau_{\text{BB}} + \tau_{\text{CC}})/T)|^2]$. Recalling the digitalized residual signal $y_{\text{R}0}(n)$ in (5) with its power being calculated as $\mathbb{E}[|y_{\text{R}0}(n)|^2] = G_{\text{P}0}^2G_{\text{FB}}^2\mathbb{E}[|y_{\text{PA}}(n - \tau_{\text{TC}}/T)|^2]$, the G_{CC} is then approximated as

$$\hat{G}_{\text{CC}} = \frac{G_{\text{P}0}G_{\text{FB}}}{G_{\text{P}2}G_{\text{BB}}} \times \sqrt{\frac{\mathbb{E}[|y_{\text{R}2}(n)|^2]}{\mathbb{E}[|y_{\text{R}0}(n)|^2]}}, \quad (20)$$

where power normalization is adopted to ensure $\mathbb{E}[|y_{\text{PA}}(n - \tau_{\text{TC}}/T)|^2] = \mathbb{E}[|x(n - (\tau_{\text{BB}} + \tau_{\text{CC}})/T)|^2]$. Therefore, the digital cancelling signal $\hat{x}(n)$ is given as

$$\hat{x}(n) = G_{\text{P}1}\hat{G}_{\text{CC}}G_{\text{BB}}x\left(n - \frac{\tau_{\text{BB}} + \hat{\tau}_{\text{CC}}}{T}\right). \quad (21)$$

3) Reconstruction: Then, by adding the digital cancelling signal given in (21) and the residual signal given in (11), an estimation of the original PA output signal is obtained as

$$\begin{aligned} y_{\text{R}}(n) &= G_{\text{P}1}y(n) - G_{\text{P}1}z(n) + \hat{x}(n) \\ &= G_{\text{P}1}G_{\text{FB}}y_{\text{PA}}\left(n - \frac{\tau_{\text{TC}}}{T}\right) - G_{\text{P}1}G_{\text{CC}}G_{\text{BB}}x\left(n - \frac{\tau_{\text{BB}} + \tau_{\text{CC}}}{T}\right) \\ &\quad + G_{\text{P}1}\hat{G}_{\text{CC}}G_{\text{BB}}x\left(n - \frac{\tau_{\text{BB}} + \hat{\tau}_{\text{CC}}}{T}\right) \\ &\approx G_{\text{P}1}G_{\text{FB}}y_{\text{PA}}\left(n - \frac{\tau_{\text{TC}}}{T}\right), \end{aligned} \quad (22)$$

where the approximation is valid due to the facts that the estimated loop delay $\hat{\tau}_{\text{CC}} \approx \tau_{\text{CC}}$ and the estimated attenuation $\hat{G}_{\text{CC}} \approx G_{\text{CC}}$. Thus, the PA output signal is recovered from the residual signal upon accurate estimations of the loop delay τ_{CC} and the attenuation G_{CC} . In Section IV, the effects of the estimation errors for τ_{CC} and G_{CC} on PA modeling and DPD linearization performance will be analyzed.

C. DPD Linearization

1) *PA Model Extraction*: Recalling the PA baseband model in (2) and denoting $\phi(n, k, q) = x(n - q)|x(n - q)|^k$, the recovered signal $y_{\text{R}}(n)$ is given as

$$y_{\text{R}}(n) = \sum_{k=0}^{K-1} \sum_{q=0}^{Q-1} w_{kq} \phi(n, k, q). \quad (23)$$

By assembling N groups of the recovered samples and the baseband PA input samples, (23) can be rewritten in a matrix form as

$$\mathbf{Y} = \Phi \mathbf{W}, \quad (24)$$

where $\mathbf{Y} = [y_{\text{R}}(0), y_{\text{R}}(1), \dots, y_{\text{R}}(N-1)]^T$ is the estimated PA output vector with N samples. $\Phi = [\Phi_0, \Phi_1, \dots, \Phi_{N-1}]^T$ is a $N \times (KQ)$ matrix constructed by $\phi(n, k, q)$, where $\Phi_n = [\phi(n, 0, 0), \dots, \phi(n, k, q), \dots, \phi(n, K-1, Q-1)]$. $\mathbf{W} = [w_{00}, \dots, w_{kq}, \dots, w_{(K-1,Q-1)}]$ is the corresponding MP model parameter vector.

By applying the least square (LS) algorithm, the solution to (24), i.e., the PA parameter estimation, is given as [4]

$$\hat{\mathbf{W}}_{\text{PA}} = (\Phi^H \Phi)^{-1} \Phi^H \mathbf{Y}, \quad (25)$$

where H denotes the complex conjugate transpose operation.

2) *DPD Model Extraction*: In the DPD coefficient estimation process, the indirect learning algorithm [21] is applied by swapping the PA input and output to estimate the DPD coefficients. Similar with (23) and (24), the input-output relationship for the DPD model can be expressed as

$$\mathbf{X} = \Psi \Omega, \quad (26)$$

where $\mathbf{X} = [x(0), x(1), \dots, x(N-1)]^T$ is the PA input vector, $\Psi = [\Psi_0, \Psi_1, \dots, \Psi_{N-1}]^T$ is a $N \times (KQ)$ matrix with $\Psi_n = [\psi(n, 0, 0), \dots, \psi(n, k, q), \dots, \psi(n, K-1, Q-1)]$ and $\psi(n, k, q) = y_{\text{R}}(n-q)|y_{\text{R}}(n-q)|^k$, and $\Omega = [\omega_{00}, \dots, \omega_{kq}, \dots, \omega_{(K-1,Q-1)}]$ is the corresponding DPD parameter vector. From (26), the DPD coefficients can also be estimated by applying the LS algorithm [4], i.e.,

$$\hat{\Omega}_{\text{DPD}} = (\Psi^H \Psi)^{-1} \Psi^H \mathbf{X}. \quad (27)$$

Subsequently, by applying the DPD linearization on the source signal $u(n)$, the predistorted source signal is represented as

$$x_{\text{DPD}}(n) = \sum_{k=0}^{K-1} \sum_{q=0}^{Q-1} \hat{\omega}_{kq} \psi_u(n, k, q), \quad (28)$$

where $\hat{\omega}_{kq}$ is the estimated DPD coefficient for k -th order and q -th memory, and $\psi_u(n, k, q) = u(n-q)|u(n-q)|^k$.

IV. PERFORMANCE ANALYSIS

As shown in Section III, the proposed architecture can reduce the ADC dynamic range requirement by approximately G_{DRI} . However, during the signal reconstruction process, due to the limited accuracy on the estimation of the delay and attenuation of the RF cancellation chain, extra errors could be introduced to the recovered PA output signal, and thus degrades the performance of the PA model extraction and the DPD linearization [33]. In the following section, the impacts of the loop delay and attenuation estimation errors on the signal reconstruction, PA model extraction, and DPD linearization are respectively analyzed. Through the analysis, the tolerance ranges for the loop delay and attenuation estimation errors can be obtained with given PA model extraction and DPD linearization performance specification, which provide restrictions for the design of the RF cancellation chain and algorithms for signal reconstruction of the proposed architecture. Thus, when the restrictions are satisfied, the impacts of the estimation errors on the DPD linearization performance can be neglected.

A. Effect on Feedback Signal Recovery

In the sequel, we utilize an OFDM system as an example to demonstrate the effects of the loop delay and attenuation estimation errors on the signal recovery, where there are N sub-carriers of frequencies separated by Δf . The duration of one OFDM symbol is $T = 1/\Delta f$. N is usually selected to be a power of two to permit the use of fast Fourier transform (FFT) routine. Then, the OFDM signal within one symbol is given as

$$\tilde{x}(t) = \frac{1}{\sqrt{N}} \sum_{l=-N/2}^{N/2-1} S_l e^{j2\pi l \Delta f t}, \quad t \in [0, T), \quad (29)$$

where S_l is the transmit symbol assigned to the l -th sub-carrier. $\tilde{x}(t)$ is generated by feeding $u(n)$ into a DAC, and thus $u(n) = \tilde{x}(nT/N)$. In the DPD feedback channel, the feedback signal from the PA output is then sampled at the rate N/T to generate $y_{\text{R}}(n)$.

The estimation errors for the loop delay and attenuation of the RF cancellation chain are quantified by δ and ρ , i.e., $\hat{G}_{\text{RC}} = G_{\text{P1}} G_{\text{CC}} (1 + \rho)$ and $\hat{\tau}_{\text{CC}} = \tau_{\text{CC}} + \delta$, where δ and ρ are modelled as random variables with zero means and variances of σ_δ^2 and σ_ρ^2 , respectively [34], [35]. After signal reconstruction, the recovered OFDM samples, impaired by the estimation errors δ and ρ , can be written as

$$\begin{aligned} y_{\text{R}}(n) &= G_{\text{P1}} y(n) - G_{\text{P1}} z(n) + \hat{x}(n) \\ &= G_{\text{P1}} G_{\text{FB}} y_{\text{PA}} \left(n - \frac{\tau_{\text{TC}}}{T} \right) - G_{\text{P1}} G_{\text{CC}} G_{\text{BB}} x \left(n - \frac{\tau_{\text{BB}} + \tau_{\text{CC}}}{T} \right) \\ &\quad + G_{\text{P1}} G_{\text{CC}} G_{\text{BB}} (1 + \rho) x \left(n - \frac{\tau_{\text{BB}} + \tau_{\text{CC}} + \delta}{T} \right). \end{aligned} \quad (30)$$

When the power $\mathbb{E}[y_{\text{R}}(n)y_{\text{R}}^*(n)]$ of the recovered signal is normalized to $G = G_{\text{P1}} G_{\text{FB}}$ and synchronized with the PA input $x(n)$, the recovered samples $y_{\text{NR}}(n)$ turns to

$$\begin{aligned} y_{\text{NR}}(n) &= \frac{G_{\text{P1}}}{G} y \left(n + \frac{\tau_{\text{TC}}}{T} \right) - \frac{G_{\text{P1}}}{G} z \left(n + \frac{\tau_{\text{TC}}}{T} \right) + \frac{1}{G} \hat{x} \left(n + \frac{\tau_{\text{TC}}}{T} \right) \\ &= y_{\text{PA}}(n) - x(n) + (1 + \rho) x \left(n - \frac{\delta}{T} \right). \end{aligned} \quad (31)$$

Define $\hat{x}_{\text{NR}}(n) = (1 + \rho)x(n - \delta/T)$, which can be expanded as

$$\begin{aligned}\hat{x}_{\text{NR}}(n) &= (1 + \rho)\frac{1}{\sqrt{N}} \sum_{l=0}^{N-1} S_l e^{j2\pi l \frac{n}{N}} e^{j2\pi l \Delta f \delta} \\ &\approx (1 + \rho)\frac{1}{\sqrt{N}} \sum_{l=0}^{N-1} S_l e^{j2\pi l \frac{n}{N}} (1 + j2\pi l \Delta f \delta),\end{aligned}$$

where the item $\exp(j2\pi l \Delta f \delta)$ can be approximated by $(1 + j2\pi l \Delta f \delta)$ since $\Delta f \delta$ is small. Then, it follows $\hat{x}_{\text{NR}}(n) \approx x(n) + \theta_x$, where θ_x is the interference introduced by the estimation error, i.e.,

$$\theta_x = \rho x(n) + (1 + \rho) \frac{j2\pi \Delta f \delta}{\sqrt{N}} \sum_{l=0}^{N-1} l S_l e^{j2\pi l \frac{n}{N}}, \quad (32)$$

with the first item being an attenuated replica of the cancelling signal and the second item being related to the transmit symbol S_l , the sub-carrier index l , the loop delay estimation error δ , and the attenuation estimation error ρ .

Therefore, the recovered PA output signal $y_{\text{NR}}(n)$ can now be written as

$$y_{\text{NR}}(n) = y_{\text{PA}}(n) + \theta_x, \quad (33)$$

and θ_x is the deviation to the exact PA output signal $y_{\text{PA}}(n)$. Without loss of generality, it is assumed that the source input symbols S_l are statistically independent and identically distributed (i.i.d.) with zero mean and variance σ_S^2 [36], i.e., $\mathbb{E}[S_l S_l^*] = \sigma_S^2$. As such, based on the central limit theorem, when the number of sub-carriers N is considerably large, the distribution of $x(n)$ approaches the Gaussian distribution with zero mean and variance $\sigma_x^2 = \sigma_S^2$ [36], [37]. Since δ and ρ are also independent with the input and feedback data streams, i.e., $\mathbb{E}[\delta x^*(n)] = 0$, it can be readily verified from (32) that $\mathbb{E}[\theta_x] = 0$ and

$$\mathbb{E}[\theta_x \theta_x^*] = \sigma_\rho^2 \sigma_S^2 + (1 + \sigma_\rho^2) \frac{4\pi^2 \sigma_\delta^2 \Delta f^2}{N} \sum_{l=0}^{N-1} l^2 \sigma_S^2. \quad (34)$$

It is observed that $\mathbb{E}[\theta_x \theta_x^*]$ is related to the variances of the loop delay and attenuation estimation errors, i.e., σ_ρ^2 and σ_δ^2 , as well as the number of subcarrier N and subcarrier frequency spacing Δf .

B. Effect on PA Model Extraction & DPD Linearization

The metric NMSE is usually utilized to evaluate the PA behavior model, which is defined by

$$\eta = \frac{\mathbb{E}[|y_{\text{meas}}(n) - y_{\text{esti}}(n)|^2]}{\mathbb{E}[|y_{\text{meas}}(n)|^2]}, \quad (35)$$

where $y_{\text{meas}}(n)$ and $y_{\text{esti}}(n)$ are the measured and estimated PA output samples, respectively. Considering the modeling errors mainly caused by the delay and attenuation estimation errors ρ and δ as well as the measurement noise $v(n)$ in the feedback

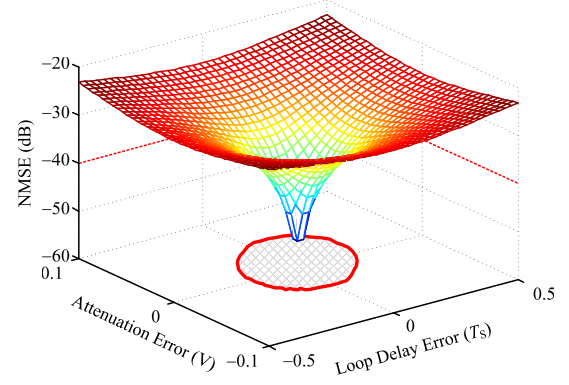


Fig. 5. NMSE performance for a 20 MHz LTE-advanced signal in terms of the loop delay and attenuation estimation errors, where the SNR of the feedback channel is set to $\gamma = 55$ dB. The dashed line shows the -40 dB NMSE performance limit. The area with diagonal cross stripes shows the ranges for σ_ρ and σ_δ where the NMSE performance is lower than -40 dB.

path, the NMSE of the PA modeling process is given as

$$\begin{aligned}\eta &= \frac{\mathbb{E}[|y_{\text{R}}(n) - y(n) + v(n)|^2]}{\mathbb{E}[|y_{\text{R}}(n)|^2]} \\ &= \frac{\mathbb{E}[|\theta_x|^2] + \mathbb{E}[|v(n)|^2] + \mathbb{E}[\theta_x v^*(n)] + \mathbb{E}[\theta_x^* v(n)]}{\mathbb{E}[|y_{\text{R}}(n)|^2]}. \quad (36)\end{aligned}$$

Since the measurement noise $v(n)$ is independent with the source signal and the feedback signal, it can be readily verified that $v(n)$ is also independent with the interference θ_x , i.e., $\mathbb{E}[\theta_x v^*(n)] = \mathbb{E}[\theta_x^* v(n)] = 0$. Given that the power of the feedback signal is normalized to that of the input signal, i.e., $\mathbb{E}[|y_{\text{d}}(n)|^2] = \mathbb{E}[|y(n)|^2] = \sigma_S^2$, the NMSE with the delay and attenuation estimation errors can be rewritten as

$$\begin{aligned}\eta &= \frac{3\sigma_\rho^2 + 2\pi^2(1 + \sigma_\rho^2)\sigma_\delta^2(2N-1)(N-1)\Delta f^2}{3} + \frac{1}{\gamma} \\ &\approx \frac{3\sigma_\rho^2 + 4\pi^2(1 + \sigma_\rho^2)\sigma_\delta^2 W^2}{3} + \frac{1}{\gamma}, \quad (37)\end{aligned}$$

where $(2N-1)(N-1)$ is approximated by $2N^2$ as N is considerably large [36], $W = N \times \Delta f$ is the transmit signal bandwidth, and $\gamma = \sigma_S^2/\sigma_v^2$ is the SNR of the feedback channel.

In the sequel, we adopt simulations to demonstrate the effects of loop delay and attenuation estimation errors on the NMSE, where δ and ρ are modeled as additive white Gaussian random variables with RMS value σ_δ of δ , with $-0.5T_s \leq \sigma_\delta \leq 0.5T_s$, and $\rho - 0.1V \leq \sigma_\rho \leq 0.1V$, respectively.

Fig. 5 shows the NMSE performance in terms of the loop delay estimation error δ and attenuation estimation error ρ for a 20 MHz LTE-advanced source signal, and Fig. 6 shows similar NMSE performance for a 40 MHz LTE-advanced signal. It is obvious that the NMSE degrades as the RMS values σ_δ and σ_ρ increase. By comparing Fig. 5 and Fig. 6, it can be concluded that as the transmission bandwidth increases, NMSE is more sensitive to the change of the loop delay

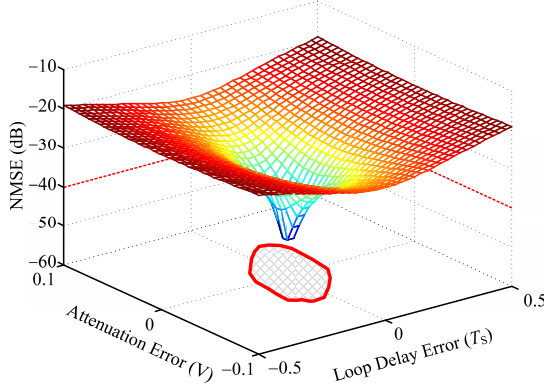


Fig. 6. NMSE performance for a 40 MHz LTE-advanced signal in terms of the loop delay and attenuation estimation errors, where the SNR of the feedback channel is set to $\gamma = 55$ dB. The dashed line shows the -40 dB NMSE performance limit. The area with diagonal cross stripes shows the effective ranges for σ_ρ and σ_δ where the NMSE performance is lower than -40 dB.

estimation error. In practice, NMSE performance is usually around -40 dB [4], [9], [11], [38]. Thus, to achieve this goal, the estimation accuracies for both the loop delay and attenuation should be controlled within certain ranges, e.g., the areas with diagonal strips in Fig. 5 and Fig. 6.

Beyond NMSE, ACLR is another metric used to evaluate the DPD linearization performance, which is defined as the ratio of the power in the main channel to the power leakage in the adjacent channel (without overlap between the channels), i.e.,

$$\begin{aligned} \xi_R &= 10 \log_{10} \left(\frac{\int_{-F_c/2}^{F_c/2} P(f) df}{\int_{F_c/2}^{3F_c/2} P(f) df} \right), \\ \xi_L &= 10 \log_{10} \left(\frac{\int_{-F_c/2}^{F_c/2} P(f) df}{\int_{-3F_c/2}^{-F_c/2} P(f) df} \right), \end{aligned} \quad (38)$$

where ξ_R is the ACLR for upper frequency offset, ξ_L is the ACLR for the lower frequency offset, $P(f)$ is the power spectral density of the PA output signal, and F_c is the bandwidth of the input signal and is equal to the chip rate multiplied by the roll-off of the shaping filter [39]. Without loss of generality, in this section, ACLR for the upper frequency offset ξ_R is used as the criteria for linearization performance evaluation.

Fig. 7 shows the ACLR performance in terms of the loop delay estimation error δ and attenuation estimation error ρ for a 20 MHz LTE-advanced source signal and Fig. 8 shows similar ACLR performance for a 40 MHz LTE-advanced signal. It is shown that δ and ρ degrade the ACLR performance, even resulting in violations of the -45 dBc requirement [25]. However, when the accuracy of the estimations for the loop delay and attenuation is controlled within reasonable ranges, e.g., the areas with diagonal strips shown in Fig. 7 and Fig. 8, ACLR performances lower than -45 dBc are preserved with ADC of less ENOB.

V. EXPERIMENTAL RESULTS

A. Setup

The experimental setup adopted to evaluate the effectiveness of the proposed DPD architecture is shown in Fig. 9, where

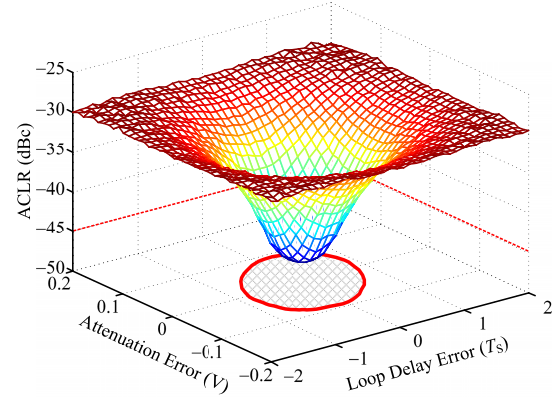


Fig. 7. Simulated ACLR performance for a 20 MHz LTE-advanced signal in terms of the loop delay and attenuation estimation errors, where the SNR of the feedback channel is set to $\gamma = 55$ dB. The dashed line shows the -45 dBc ACLR performance limit as required by the specification [25]. The area with diagonal cross stripes shows the effective ranges for σ_ρ and σ_δ where the ACLR performance meet the specification requirement.

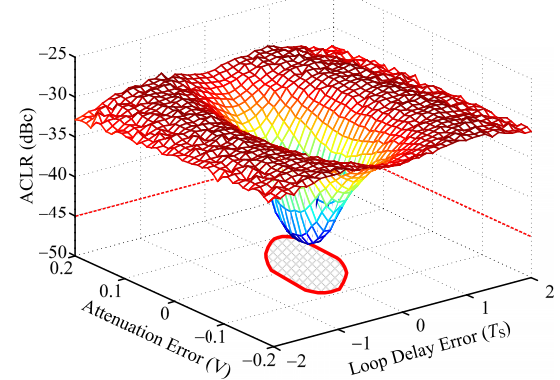
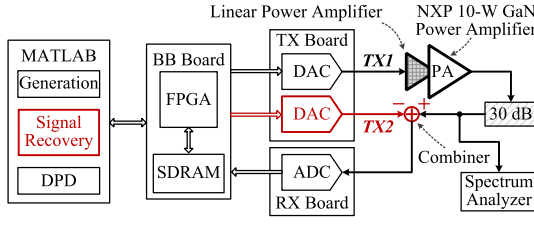


Fig. 8. Simulated ACLR performance for the 40 MHz LTE-advanced signal in terms of the loop delay and attenuation estimation errors, where the SNR of the feedback channel is set to $\gamma = 55$ dB. The dashed line shows the -45 dBc ACLR performance limit as required by the specification [25]. The area with diagonal cross stripes shows the effective ranges for σ_ρ and σ_δ where the ACLR performance meet the specification requirement.

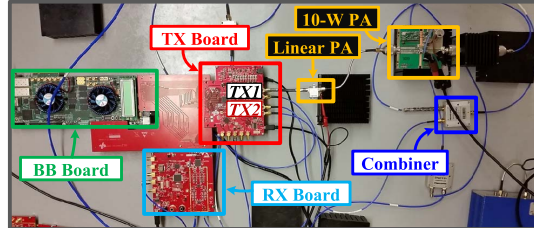
Fig. 9 (a) and Fig. 9 (b) present the systematic scheme and the photograph of the experiment, respectively. MATLAB is used to generate the baseband LTE-advanced signals, which are sent to the baseband (BB) board via a USB cable and temporarily stored at the synchronous dynamic random access memory (SDRAM) chips integrated on the BB board. The stored baseband signals are processed by the field programmable gate array (FPGA) chip (Arria V GX-360KLE FPGA) to feed the transmitting board to generate the RF signal.

A 1-Watt PA with high linearity (driver amplifier provided by Mini-Circuits) is adopted to amplify the RF signal to stimulate the main amplifier that followed. The main amplifier is a broadband class-AB PA of 10-Watts peak power, implemented with a NXP Semiconductor GaN HEMT transistor CLF1G0060-10.

In order to test the effectiveness and efficiency enhancement of the proposed DPD architecture, the BB board and the TX board are both configured to work in the dual-channel



(a) Experimental setup diagram



(b) Photograph of the experiment

Fig. 9. Setup and photograph of the experiment.

mode, i.e., one channel for transmitting and the other for RF cancellation. As illustrated in Fig. 9 (a), transmitter **TX1** is used as the transmit chain, while transmitter **TX2** is used as the RF cancellation chain. Due to the high similarity between the two transmitters, it can generate a RF cancelling signal that is almost identical to the PA amplified signal but with a 180-degree phase shift by tuning the amplitude and delay of the cancelling signal in digital domain.

The PA amplified signal and the cancelling signal are redirected to a RF power combiner to perform the RF cancellation. The residual signal of the RF cancellation is subsequently routed to the receiver board TI TSW1266 to be down-converted, digitalized, and stored in the SDRAM memory. Meanwhile, a spectrum analyzer is also attached to the attenuated PA output port for monitoring the spectrum of the output signal.

After the RF signal cancellation, the residual signal are subsequently sent back to MATLAB to be further processed and aligned with the baseband input signal to recover the PA output signal. Then, the indirect learning method is applied to the recovered signal and the baseband input signal to extract the PA model and the DPD coefficients.

B. Procedure

The experiments are carried out in two phases: the testing phase and the validating phase. In the testing phase, two LTE-advanced signals with 20 MHz and 40 MHz bandwidth are both used to verify the PA modeling and DPD linearization performance under the proposed architecture with the cancellation and reconstruction operation. NMSE and ACLR are adopted as two metrics to compare the performance of the proposed architecture and the conventional DPD as discussed in [4]. During the RF signal cancellation, τ_{BB} and G_{BB} are tuned to cancel the PA output signal by 15.0 dB and 26.3 dB (the maximum value we can achieve in the experiments). Correspondingly, the ENOB required to capture the residual signal are reduced by about $15/6.02 \approx 2.5$ bits

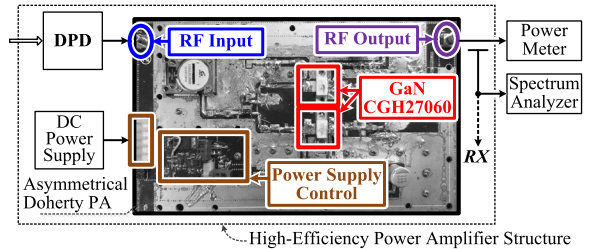


Fig. 10. A systematic architecture of the high-efficiency PA used to validate the efficiency improvement of the proposed DPD architecture.

TABLE I
NMSE AND ACLR PERFORMANCE FOR LTE-ADVANCED SIGNALS
WITH DIFFERENT DPD ARCHITECTURES

Source	DPD Methods	NMSE	ACLR (+/-)*	ADC-Bits
20 MHz	Without DPD	-29.1 dB	-31.2/-30.6 dBc	12
		-40.2 dB	-51.3/-50.7 dBc	12
	Conv. DPD [14]	-40.1 dB	-50.6/-50.2 dBc	10
		-37.4 dB	-46.1/-46.0 dBc	8
40 MHz	Proposed DPD	-39.6 dB	-50.1/-49.3 dBc	10
		-39.3 dB	-49.2/-48.9 dBc	8
	Without DPD	-28.0 dB	-29.7/-29.1 dBc	12
		-39.7 dB	-50.1/-49.5 dBc	12
40 MHz	Conv. DPD [14]	-39.1 dB	-48.0/-49.2 dBc	10
		-36.3 dB	-44.2/-45.4 dBc	8
	Proposed DPD	-38.9 dB	-48.7/-48.1 dBc	10
		-38.7 dB	-47.6/-47.9 dBc	8

* The ACLR is measured with +/-20MHz frequency offsets for both the 20-MHz and 40-MHz LTE-advanced signals.

and $26.3/6.02 \approx 4.4$ bits, respectively. In order to simulate the characteristics of a 10-bit ADC and a 8-bit ADC in the digital domain, only the lower 10 and 8 bits of the 12-bit ADC ADS5402 are respectively used to acquire the residual signals.

In the validating phase, in order to further validate the efficiency improvement, a Doherty PA with 50 dBm saturation power based on the classical asymmetrical structure [8] is fabricated and adopted in the experiments. As shown in Fig. 10, the Doherty PA is constructed by two GaN CGH27060 transistors working at 2.35 GHz. A 40 MHz LTE-advanced signal is used as the RF input signal to be amplified to different output power levels. For each output power level, the ACLR performance is measured by the spectrum analyzer at the RF output port, and the power added efficiency (PAE), which is a metric for rating the power efficiency of a PA, is calculated by monitoring the drain current and voltage of the direct current (DC) power supply for the Doherty PA as well as the gain of PA.

C. Testing Results

Table I compares the NMSE and ACLR performance of the proposed DPD architecture with the conventional DPD structure in [4], with different ADC resolution bits being used. It is observed that the NMSE performance of the proposed DPD is quite close to those of the conventional DPD for both the 20 MHz and 40 MHz LTE-advanced signals, i.e., the modeling error introduced by the proposed cancellation and reconstruction mechanism can be neglected. This result is

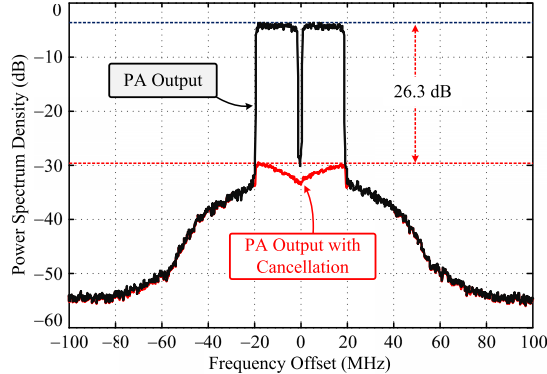


Fig. 11. The RF cancellation result a 40 MHz LTE-advanced signal.

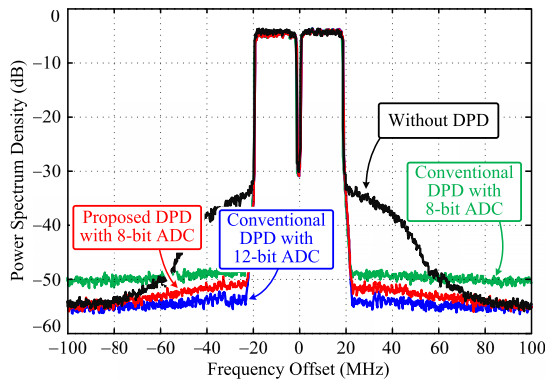


Fig. 12. DPD linearization results for a 40 MHz LTE-advanced signal, where in the proposed DPD architecture an signal cancellation amount of 26.3 dB is achieved and only the lower 8 bits of the ADC are adopted for signal sampling.

consistent with the analytical results in (37) and the simulation results shown in Fig. 5 and Fig. 6. The ACLR performance of the proposed DPD is at least 2.6 dB above the -45 dBc ACLR limit for both the 20 MHz and 40 MHz source signals, whereas the ACLR performance of the conventional DPD dramatically degrades as the ADC resolution bits are reduced. Specifically, when an 8-bit ADC is used to acquire the 40 MHz LTE-advanced signal, an ACLR of -47.6 dBc is achieved with the proposed DPD architecture, which outperforms the conventional DPD [4] by about 3.4 dB.

Fig. 11 shows the spectra of the PA outputs with and without the proposed RF signal cancellation. In this experiment, a maximum cancellation amount of 26.3 dB is achieved, which thereby provides 26.3 dB dynamic range improvement, i.e., a resolution redundancy of $26.3/6.02 \approx 4.4$ bits for ADC, and is consistent with the simulation results in Fig. 4. In this case, only an 8-bit ADC is required to acquire the residual signal. It is demonstrated in Fig. 12 that the proposed DPD linearization with 8-bit ADC also provides an effective suppression of the spectra regrowth caused by the PA nonlinearities. Whereas the conventional DPD with 8-bit ADC violates the -45 dBc ACLR requirement by about 0.8 dB.

D. Power Efficiency Improvement

Fig. 13 shows the ACLR performance measured at the Doherty PA output with power level ranging from 26.5 dBm

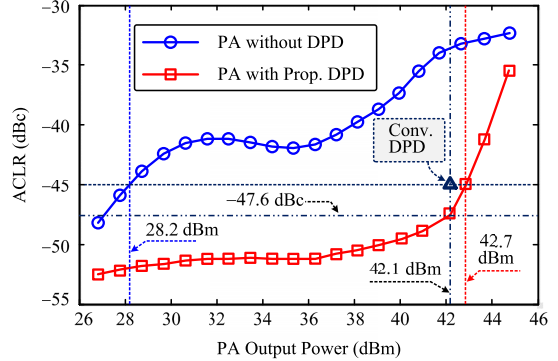


Fig. 13. Measured ACLR performance versus PA output power level for a 40 MHz LTE-advanced signal.

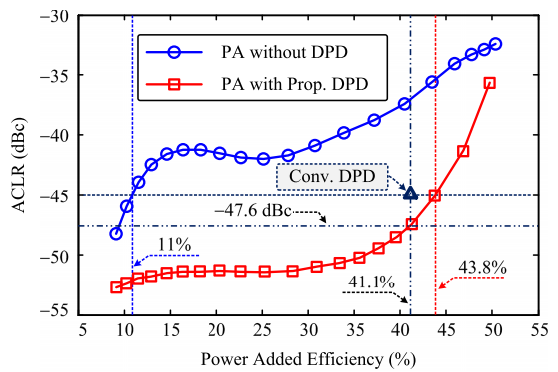


Fig. 14. Measured ACLR performance versus PAE for a 40 MHz LTE-advanced signal.

to 44.5 dBm. With the proposed DPD linearization, the ACLR performance is significantly improved within a wide PA output power range (as the output power increases, it is more difficult to improve the ACLR performance). Specifically, the Doherty amplifier without DPD linearization can only provide an output power of 28.2 dBm to satisfy the -45 dBc ACLR requirement for BSs [25]. In such a case, a 21.8 dB power back-off from the 50 dBm saturation power must be applied to this amplifier. By applying the conventional DPD method with an 8-bit ADC to acquire the feedback signal, the output power level of the PA can only be increased to 42.1 dBm to satisfy the ACLR requirement. As a comparison, the proposed DPD linearization gives an ACLR of about -47.6 dBc at the same output power level of -42.1 dBm (16.2 Watts), which provides approximately 2.6 dB ACLR margin to further increase the PA output power level by 14.8% to 42.7 dBm (18.6 Watts).

As shown in Fig. 14, due to the 21.8 dB power back-off, the PAE of the Doherty PA without DPD linearization is dramatically reduced to about 11%. By applying the conventional DPD method, the PAE is increased to about 41.1% with 7.9 dB back-off power. When the proposed DPD architecture is applied, the PAE is further improved to 43.8% with only 7.3 dB back-off power, which respectively provides about 32.8% and 2.7% efficiency improvements over the Doherty amplifier without DPD linearization and the conventional DPD method.

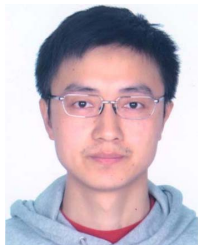
VI. CONCLUSION

In this paper, a novel DPD architecture was proposed to effectively compensate for the nonlinear distortion in wideband PA with limited ADC dynamic range. By introducing an extra RF cancellation chain, the linear component of the PA amplified signal was first eliminated before entering the ADC to reduce the signal dynamic range. Then, the loop delay and attenuation introduced by the RF cancellation chain were estimated to generate the baseband replica of the RF cancelling signal, which was subsequently added onto the digitalized residual signal to estimate the original PA output signal. Finally, the estimated PA output and the PA input signals were used with an indirect learning structure to extract the DPD model, which could be applied in a wireless transmitter to counteract the nonlinear distortion caused by the PA. Experiments demonstrated the effectiveness of the proposed DPD architecture with both 20 MHz and 40 MHz LTE-advanced signals. It was observed that the proposed DPD architecture could improve the ADC dynamic range by up to 26.3 dB, which equivalently reduced the ADC resolution by approximately 4.4 bits, with a superior ACLR over the conventional DPD by about 3.4 dB. By further applying this DPD architecture to a widely-used Doherty amplifier with 50 dBm saturation power, a power added efficiency of 43.8% was achieved with only 7.3 dB back-off power, which respectively demonstrates 32.8% and 2.7% efficiency improvements at an output power level of 42.7 dBm with -45 dBc ACLR performance, compared to the one applying power back-off only and the conventional DPD method. Thus, this novel DPD architecture could provide a solution for wide-band PA linearization, particularly when stringent requirements are placed on the ADC dynamic range.

REFERENCES

- [1] Z. Shen, A. Papasakellariou, J. Montojo, D. Gerstenberger, and F. Xu, "Overview of 3GPP LTE-advanced carrier aggregation for 4G wireless communications," *IEEE Commun. Mag.*, vol. 50, no. 2, pp. 122–130, Feb. 2012.
- [2] H. Ochiai and H. Imai, "On the distribution of the peak-to-average power ratio in OFDM signals," *IEEE Trans. Commun.*, vol. 49, no. 2, pp. 282–289, Feb. 2001.
- [3] L. Guan and A. Zhu, "Green communications: Digital predistortion for wideband RF power amplifiers," *IEEE Microw. Mag.*, vol. 15, no. 7, pp. 84–99, Nov./Dec. 2014.
- [4] L. Ding *et al.*, "A robust digital baseband predistorter constructed using memory polynomials," *IEEE Trans. Commun.*, vol. 52, no. 1, pp. 159–165, Jan. 2004.
- [5] H. Bogucka and A. Conti, "Degrees of freedom for energy savings in practical adaptive wireless systems," *IEEE Commun. Mag.*, vol. 49, no. 6, pp. 38–45, Jun. 2011.
- [6] M. J. Pelk, W. C. E. Neo, J. R. Gajadharasing, R. S. Pengelly, and L. C. N. de Vreede, "A high-efficiency 100-W GaN three-way Doherty amplifier for base-station applications," *IEEE Trans. Microw. Theory Techn.*, vol. 56, no. 7, pp. 1582–1591, Jul. 2008.
- [7] J. Xia, X. Zhu, L. Zhang, J. Zhai, and Y. Sun, "High-efficiency GaN Doherty power amplifier for 100-MHz LTE-advanced application based on modified load modulation network," *IEEE Trans. Microw. Theory Techn.*, vol. 61, no. 8, pp. 2911–2921, Aug. 2013.
- [8] J. Kim, J. Cha, I. Kim, and B. Kim, "Optimum operation of asymmetrical-cells-based linear Doherty power amplifiers-uneven power drive and power matching," *IEEE Trans. Microw. Theory Techn.*, vol. 53, no. 5, pp. 1802–1809, May 2005.
- [9] Y. Liu, W. Pan, S. Shao, and Y. Tang, "A general digital predistortion architecture using constrained feedback bandwidth for wideband power amplifiers," *IEEE Trans. Microw. Theory Techn.*, vol. 63, no. 5, pp. 1544–1555, May 2015.
- [10] P. Roblin, C. Quindroit, N. Naraharisetti, S. Gheitanchi, and M. Fitton, "Concurrent linearization: The state of the art for modeling and linearization of multiband power amplifiers," *IEEE Microw. Mag.*, vol. 14, no. 7, pp. 75–91, Nov./Dec. 2013.
- [11] Y. Liu, W. Pan, S. Shao, and Y. Tang, "A new digital predistortion for wideband power amplifiers with constrained feedback bandwidth," *IEEE Microw. Wireless Compon. Lett.*, vol. 23, no. 12, pp. 683–685, Dec. 2013.
- [12] Y. Liu, J. Y. Yan, H. T. Dabag, and P. M. Asbeck, "Novel technique for wideband digital predistortion of power amplifiers with an undersampling ADC," *IEEE Trans. Microw. Theory Techn.*, vol. 62, no. 11, pp. 2604–2617, Nov. 2014.
- [13] G. Su, W. Chen, S. Zhang, and F. M. Ghannouchi, "A robust and low sampling rate digital predistortion algorithm for broadband PA modeling and predistortion," in *Proc. 15th Annu. Wireless Microw. Technol. Conf. (WAMICON)*, Tampa, FL, USA, Jun. 2014, pp. 1–4.
- [14] *ADC12D800/500RF 12-Bit, 1.6/1.0 GSPS RF Sampling ADC*, Texas Instruments Inc., Dallas, TX, USA, Mar. 2013.
- [15] *ADC08D500 High Performance, Low Power, Dual 8-Bit, 500 MSPS A/D Converter*, Texas Instruments Inc., Dallas, TX, USA, Apr. 2013.
- [16] L. Bin, T. W. Rondeau, J. H. Reed, and C. W. Bostian, "Analog-to-digital converters," *IEEE Signal Process. Mag.*, vol. 22, no. 6, pp. 69–77, Nov. 2005.
- [17] C. Yu, L. Guan, E. Zhu, and A. Zhu, "Band-limited Volterra series-based digital predistortion for wideband RF power amplifiers," *IEEE Trans. Microw. Theory Techn.*, vol. 60, no. 12, pp. 4198–4208, Dec. 2012.
- [18] Y. Y. Woo *et al.*, "Adaptive digital feedback predistortion technique for linearizing power amplifiers," *IEEE Trans. Microw. Theory Techn.*, vol. 55, no. 5, pp. 932–940, May 2007.
- [19] L. Sundstrom, M. Faulkner, and M. Johansson, "Quantization analysis and design of a digital predistortion linearizer for RF power amplifiers," *IEEE Trans. Veh. Technol.*, vol. 45, no. 4, pp. 707–719, Nov. 1996.
- [20] J. Wood, "Digital pre-distortion of RF power amplifiers: Progress to date and future challenges," in *Proc. IEEE MTT-S Int. Microw. Symp.*, Tampa, FL, USA, May 2015, pp. 1–3.
- [21] C. Eun and E. J. Powers, "A new Volterra predistorter based on the indirect learning architecture," *IEEE Trans. Signal Process.*, vol. 45, no. 1, pp. 223–227, Jan. 1997.
- [22] S. K. Mitra, *Digital Signal Processing: A Computer-Based Approach*, 2nd ed. New York, NY, USA: McGraw-Hill, 2001.
- [23] M. I. Skolnik, *Introduction to Radar Systems*, 3rd ed. New York, NY, USA: McGraw-Hill, 2001.
- [24] *GSM Specification: Radio Transmission and Reception*, GSM 05.05 version 8.5.1, ETSI EN 300 910, Nov. 2000 [Online]. Available: <http://www.etsi.org>
- [25] *E-UTRA Base Station (BS) Radio Transmission and Reception (Release 11)*, 3GPP TS Standard 36.104, version 11.3.1, Feb. 2013.
- [26] M. Rawat, P. Roblin, C. Quindroit, K. Salam, and C. Xie, "Concurrent dual-band modeling and digital predistortion in the presence of unfilterable harmonic signal interference," *IEEE Trans. Microw. Theory Techn.*, vol. 63, no. 2, pp. 625–637, Feb. 2015.
- [27] M. Jain *et al.*, "Practical, real-time, full duplex wireless," in *Proc. Annu. Int. Conf. Mobile Comput. Netw. (ACM MobiCom)*, Las Vegas, NV, USA, Sep. 2011, pp. 301–312.
- [28] S. Tang, K. Gong, J. Wang, K. Peng, C. Pan, and Z. Yang, "Loop delay correction for adaptive digital linearization of power amplifiers," in *Proc. IEEE Wireless Commun. Netw. Conf. (WCNC)*, Hong Kong, Mar. 2007, pp. 1987–1990.
- [29] M. Duarte, C. Dick, and A. Sabharwal, "Experiment-driven characterization of full-duplex wireless systems," *IEEE Trans. Wireless Commun.*, vol. 11, no. 12, pp. 4296–4307, Dec. 2012.
- [30] D. Korpi, T. Riihonen, V. Syrjälä, L. Anttila, M. Valkama, and R. Wichman, "Full-duplex transceiver system calculations: Analysis of ADC and linearity challenges," *IEEE Trans. Wireless Commun.*, vol. 13, no. 17, pp. 3821–3836, Jul. 2014.
- [31] B. P. Day, A. R. Margetts, D. W. Bliss, and P. Schniter, "Full-duplex MIMO relaying: Achievable rates under limited dynamic range," *IEEE J. Sel. Areas Commun.*, vol. 30, no. 8, pp. 1541–1553, Sep. 2012.
- [32] R. Raich, H. Qian, and G. T. Zhou, "Orthogonal polynomials for power amplifier modeling and predistorter design," *IEEE Trans. Veh. Technol.*, vol. 53, no. 5, pp. 1468–1479, Sep. 2004.
- [33] U. Onunkwo, Y. Li, and A. Swami, "Effect of timing jitter on OFDM-based UWB systems," *IEEE J. Sel. Areas Commun.*, vol. 24, no. 4, pp. 787–793, Apr. 2006.
- [34] Z. J. Towfic, S. K. Ting, and A. H. Sayed, "Clock jitter compensation in high-rate ADC circuits," *IEEE Trans. Signal Process.*, vol. 60, no. 11, pp. 5738–5753, Nov. 2012.

- [35] Y. Liu, W. Pan, S. Shao, C. Qing, and Y. Tang, "The effect of feedback sampling clock jitter on the performance of direct learning digital predistortion in wideband systems," *IEEE Wireless Commun. Lett.*, vol. 2, no. 5, pp. 479–482, Oct. 2013.
- [36] T. Jiang and Y. Wu, "An overview: Peak-to-average power ratio reduction techniques for OFDM signals," *IEEE Trans. Broadcast.*, vol. 54, no. 2, pp. 257–268, Jun. 2008.
- [37] N. Y. Ermolova and O. Tirkkonen, "Theoretical characterization of memory polynomial models with Gaussian inputs," *IEEE Signal Process. Lett.*, vol. 16, no. 8, pp. 651–654, Aug. 2009.
- [38] D. R. Morgan, Z. Ma, J. Kim, M. G. Zierdt, and J. Pastalan, "A generalized memory polynomial model for digital predistortion of RF power amplifiers," *IEEE Trans. Signal Process.*, vol. 54, no. 10, pp. 3852–3860, Oct. 2006.
- [39] P. Jardin and G. Baudoin, "Filter lookup table method for power amplifier linearization," *IEEE Trans. Veh. Technol.*, vol. 56, no. 3, pp. 1076–1087, May 2007.



Ying Liu (S'13–M'16) received the B.E. and M.S. degrees in communication engineering and the Ph.D. degree in communication and information systems from the University of Electronic Science and Technology of China (UESTC) in 2008, 2011, and 2016, respectively. He had also worked as a Visiting Scholar with the Department of Electrical and Computer Engineering, The Ohio State University, Columbus, OH, USA. He is currently a Post-Doctoral Researcher with the School of Electronic Engineering, UESTC. His research interests include nonlinear modeling, digital predistortion, full duplex communications, and signal processing in wireless communications.



Chuang Huang (S'09–M'13) received the B.S. degree in mathematics and the M.S. degree in communications engineering from the University of Electronic Science and Technology of China, Chengdu, and the Ph.D. degree in electrical engineering from Texas A&M University, College Station, TX, USA, in 2012. From 2012 to 2013, he was a Post-Doctoral Research Fellow, and was an Assistant Research Professor from 2013 to 2014 with Arizona State University, Tempe, AZ, USA. He had also worked as a Visiting Scholar with the National University of Singapore and as a Research Associate with Princeton University, respectively. He is currently with the National Key Laboratory of Science and Technology on Communications, University of Electronic Science and Technology of China. He is now serving as an Editor of IEEE ACCESS, and was a TPC member for many IEEE conferences. His current research interests include energy harvesting communications, multicast traffic scheduling, full duplex communications, and signal processing in wireless communications.



Xin Quan (S'13) was born in Hebei, China, in 1988. She received the B.E. degree in communication engineering from Yan'an University, Qinhuangdao, China, in 2010, and the M.S. degree in communication and information systems from the University of Science and Technology of China, Chengdu, China, in 2013, where she is currently pursuing the Ph.D. degree in communication and information system with the National Key Laboratory of Science and Technology on Communications. She had worked as a Visiting Scholar with the Department of Electrical and Computer Engineering, The Ohio State University, Columbus, OH, USA. Her research interests include channel estimation, interference suppression, full duplex, and signal processing in wireless communications.



Patrick Roblin (M'85–SM'14) received the Maîtrise de Physics degree from Louis Pasteur University, Strasbourg, France, in 1980, and the M.S. and D.Sc. degrees in electrical engineering from Washington University, St. Louis, MO, USA, in 1982 and 1984, respectively. In 1984, he joined the Department of Electrical Engineering, The Ohio State University (OSU), Columbus, OH, USA, as an Assistant Professor and is currently a Professor. His current research interests include the measurement, modeling, design, and linearization of nonlinear RF devices and circuits, such as oscillators, mixers, and power amplifiers. He is the first author of two textbooks entitled *High-Speed Heterostructure and Devices* (Cambridge University Press, 2002) and *Nonlinear RF Circuits and Nonlinear Vector Network Analyzers* (Cambridge University Press, 2011). At OSU, he is the Founder of the Non-Linear RF Research Laboratory. He has developed two educational RF/microwave laboratories and associated curriculum for training both undergraduate and graduate students.



Wensheng Pan was born in Chongqing, China, in 1975. He received the B.E. and M.S. degrees in communication engineering from the University of Science and Technology of China in 1998 and 2005, respectively, where he is currently pursuing the Ph.D. degree with the Key Lab of Science and Technology on Communications. He served as a Manager with NtSTechnology Inc., from 2005 to 2009. His research interests include power amplifier design, power amplifier linearization, digital predistortion, and crest factor reduction.



Youxi Tang was born in Henan, China, in 1964. He received the B.E. degree in radar engineering from the College of PLA Ordnance, Shijiazhuang, China, in 1985, and the M.S. and Ph.D. degrees in communications and information systems from the University of Electronic Science and Technology of China, Chengdu, China, in 1993 and 1997, respectively. From 1998 to 2000, he was with Huawei Technologies Company Ltd., Shanghai, China, as a Program Manager, working in the area of IS-95 mobile communications and third-generation mobile communications. Since 2000, he has been with the National Key Laboratory of Science and Technology on Communications, University of Electronic Science and Technology of China, as a Professor. His general research interests include spread spectrum systems and wireless mobile systems with emphasis on signal processing in communications.